Density of states for dilute nitride systems: calculation of lifetime broadening

2009 J. Phys.: Condens. Matter 21 255801

(http://iopscience.iop.org/0953-8984/21/25/255801)

IOP PUBLISHING JOURNAL OF PHYSICS: CONDENSED MATTER

J. Phys.: Condens. Matter **21** (2009) 255801 (7pp) doi:10.1088/0953-8984/21/25/255801

Density of states for dilute nitride systems: calculation of lifetime broadening

N Vogiatzis and J M Rorison

Centre for Communications Research, Electrical and Electronic Engineering,
Merchant Venturers Building, Woodland Road, University of Bristol, Bristol, UK

E-mail: Nik.Vogiatzis@bristol.ac.uk and Judy.Rorison@bristol.ac.uk

Received 16 March 2009, in final form 7 May 2009
Published 27 May 2009
Online at stacks.iop.org/JPhysCM/21/255801

Abstract

We present calculations for the band structure of bulk and confined quantum well and quantum wire GaInNAs structures. To treat this non-randomly alloyed material system we follow previous approaches in using an Anderson impurity model where the nitrogen localized states interact with the GaInAs conduction band states. We solve this model using Matsubara Green's functions and the associated self-energies which produce a complex band structure where both the real and imaginary components depend on the concentration of nitrogen. In particular this approach gives a definite nitrogen dependent lifetime broadening and is different from previous work in that no artificial input parameters are used. The density of states of the conduction band, derived from these functions, is strongly altered by interaction with the nitrogen states. The density of states is required for further optical and transport investigations involving this system.

(Some figures in this article are in colour only in the electronic version)

1. Introduction

GaInNAs and GaInNAs/GaAs confined structures, quantum wells (QWs) and quantum wires (QWWs), are promising material systems for long wavelength region applications [1]. Nitrogen's high electronegativity and small atomic radius cause a strong perturbation of the host matrix resulting in a large bowing parameter and in an increase in nonparabolicity of the effective mass. The large bandgap reduction experimentally observed by Weyers *et al* [2] was explained later by the band anti-crossing (BAC) effect [3], assuming that the nitrogen localized state interacts with the InGaAs conduction band state. When the number of nitrogen atoms increases, nitrogen pair states were observed by Liu *et al* [4]. These and higher order cluster states which are statistically distributed into the host crystal were also shown later through LCINS calculations [5]. A 3×3 Hamiltonian incorporating a N–N pair state has been introduced [6] which allows interaction with one other state. More detailed information can be obtained by the empirical pseudopotential method (EPM) [7] and by tight-binding calculations [8].

Despite the huge popularity of the BAC model, it fails to provide sufficient information on the nature of the resultant mixed states. This has been considered by Wu *et al* [12] and Vaughan and Ridley [13], where Green's functions were used to describe the conduction band states after mixing. In these treatments, the broadening of the impurity states was dependent upon the density of states (DOS) of the host matrix, which was essentially taken as constant. In the current approach a nitrogen concentration dependence of the broadening of the impurity states is derived, which results in a different expression for their energy shift. This approach can also be used to calculate the density of states required for optical and transport analysis [10, 11]. Despite the different approximation, we show that all these quantities are in general agreement with those in [12, 13].

Throughout this work we consider two impurity energy levels. The first level represents single N atoms and the second an averaged N–N pair and cluster energy state distribution. While the energy of the single N level is fixed relative to the conduction band minima, the energy of the N pair and cluster states spans a distribution of energies reflecting different site distributions and other factors which will depend upon growth. To understand the importance of the energy distribution of the pair/cluster states we model it by a mean, in various energy positions within the calculated distribution spectrum.

In section 2 we present the model and results for the impurity and conduction band states, before and after mixing. In section 3 the density of states are derived based on the previous assumptions. In section 4 of the paper, we discuss

the implications that the alternate shape of the density of states may have in transport analysis in dilute nitrides.

2. The model

When non-interacting electrons of InGaAs conduction band (extended $|s\rangle$ states), interact with more than one nitrogen impurity state, one extends from the single impurity Anderson model (SIAM) [14] to the many impurity Anderson model (MIAM). In this case the Hamiltonian is

$$H = H_o + H' \tag{1}$$

where H_o is the Hamiltonian of the non-interacting system given by

$$H_o = \sum_{\mathrm{k}} \varepsilon^{\mathrm{c}}_{\mathrm{k}} \hat{c}^{\dagger}_{\mathrm{k}} \hat{c}_{\mathrm{k}} + \sum_{j} \varepsilon_j \hat{b}^{\dagger}_j \hat{b}_j \tag{2}$$

where $\varepsilon^{\mathrm{c}}_{\mathrm{k}}$ represents the extended $|s\rangle$ states and ε_j is the energy level of the jth impurity state. The $c^{(\dagger)}_{\mathrm{k}}$, $b^{(\dagger)}_j$ are the creation (annihilation) operators of the extended and localized states respectively. The second term in equation (1) describes the interaction of the conduction band and the localized states as follows:

$$H' = \sum_{j,\mathrm{k}} V_{\mathrm{k}j} (\hat{b}^{\dagger}_j \hat{c}_{\mathrm{k}} + \hat{c}^{\dagger}_{\mathrm{k}} \hat{b}_j) \tag{3}$$

where $V_{\mathrm{k}j}$ describes interaction strength of a free electron with the jth impurity level. In the MIAM each impurity energy level interacts with the conduction band independently of other impurity states and the impurity states do not mix with each other.

2.1. Method of solution: the localized state—general

In order to obtain the retarded Green's functions for solving equation (1), the Matsubara functions of imaginary frequency [9] are used. For the localized states we have

$$G_j(\mathrm{i}\hbar\omega) = \{\mathrm{i}\hbar\omega - \epsilon_j - \Sigma_{\mathrm{ret}}(\mathrm{i}\hbar\omega)\}^{-1} \tag{4}$$

where $\Sigma_{\mathrm{ret}}(\mathrm{i}\hbar\omega) = V_j^2 \sum_{\mathrm{k}} {}_{\mathrm{ret}}(\mathrm{i}\hbar\omega - \varepsilon^{\mathrm{c}}_{\mathrm{k}})$ the retarded self-energy. The subscript **k** has been suppressed in the interaction term V_j^2 assuming that it is independent of the reciprocal vector. In this equation we have made the following assumptions, upon which the results throughout the paper will depend.

Our model follows the approach of O'Reilly *et al* [6, 8, 22], for the formulation of the interaction term V_j and also of the N levels j that will be dependent on the nitrogen concentration and on the Γ–L valley energy separation. Also, the results in this paper take the spatially averaged value for the interaction term [12], which is dependent on the conduction band wavefunction intensity on the nitrogen site. We comment in the conclusions on the effect that this approximation will have for each confined structure. The last approximation which differentiates our approach from previous work, is multiple scattering from the same impurity, which is expected to be dominant in a dilute impurity system, as the one examined here. All multiple scatterings from one impurity can be summed into a closed expression [8, 9] (which includes the self-energy of equation (4)) and then the scattering can be summed over all scattering centres. Therefore, the total scattering that arises has nitrogen concentration dependence. In this way we are able to relate the magnitude of the imaginary components which will be calculated next, to the nitrogen concentration. Here we have tacitly neglected any change of the self-energy of an impurity in the presence of another one. These additional terms that would have to enter the self-energy in Feynmann 'crossed diagrams', can be neglected.

Therefore, since scattering processes are independent, the Green's function for each $|j\rangle$ state is

$$\begin{aligned} G_j(\mathrm{i}\hbar\omega) &= \lim_{\delta\to 0^+} \left\{ \hbar\omega - \epsilon_j - \frac{V_j^2}{\hbar\omega - \varepsilon^{\mathrm{c}}_{\mathrm{k}} + \mathrm{i}\delta} \right\}^{-1} \\ &= \{\hbar\omega - \epsilon_j - [\Lambda_j(\hbar\omega) + \mathrm{i}\Delta_j(\hbar\omega)]\}^{-1} \end{aligned} \tag{5}$$

where $\Lambda_j(\hbar\omega) = \mathrm{Re}\{\Sigma_{\mathrm{ret}}(\hbar\omega)\}$, $\Delta_j(\hbar\omega) = \mathrm{Im}\{\Sigma_{\mathrm{ret}}(\hbar\omega)\}$ and $\delta < 2$ meV in our calculations. To evaluate this expression we need details of the energy dispersion of the conduction band which is compositional and confinement dependent. We assume that the conduction band is parabolic with a constant effective mass so only the confinement energy is different between the bulk, QW and QWW cases. The compositionally dependent conduction band [19] is fit analytically, for all three cases discussed and has the form $R(k) = C_a + C_f \sin\frac{k\pi}{\alpha} + C_b \cos\frac{k\pi}{\alpha}$, for $k > 0$, where α is the lattice constant and C_a, C_b, C_f other fitting constants [21]. In the previous equation, the second term can be omitted as $C_b \gg C_f$ which means that $R(k)$ continues to vary parabolically with small k.

2.2. Method of solution: the localized state—QW $Ga_{1-x}In_xN_yAs_{1-y}$/GaAs case

Using the parameterization for the conduction band [21] an analytic expression for the total retarded self-energy for each impurity will be given for $k_{\parallel} > 0$ by

$$\Sigma_{\mathrm{ret}}(\hbar\omega) = y_j \lim_{\delta\to 0^+} \frac{1}{k_1} \int_0^{k_1} \mathrm{d}k_{\parallel} \frac{\beta_j^2}{\hbar\omega - R(k_{\parallel}) + \mathrm{i}\delta} \tag{6}$$

where $\beta_j y_j^{1/2} = V_j$ [5], y_j is the concentration of the jth impurity type and $k_1 = \pi/30$ Å^{-1} which corresponds to an energy of $\hbar\omega$ =1.9 eV. In principle k_1 can be bigger but the respective energies of interest are given for the above value. Solution of equation (6) is complex. The real part when $C_f \to 0$ and $\delta \to 0^+$ is given by

$$\Lambda_j(\hbar\omega) = \begin{cases} \dfrac{\alpha V_j^2}{\pi\sqrt{\tau}_1} \left\{ \log\left(\dfrac{(1+\cos\frac{k_1\pi}{\alpha}) + \lambda \sin\frac{k_1\pi}{\alpha}}{(1+\cos\frac{k_1\pi}{\alpha}) - \lambda \sin\frac{k_1\pi}{\alpha}} \right) \right\} \\ \qquad \text{if } \varepsilon_{\mathrm{CBM}} \leqslant \hbar\omega \leqslant \varepsilon_{\mathrm{CBM}} + \dfrac{\hbar^2 k_1^2}{2m_{\mathrm{eff}}} \\ \dfrac{\alpha V_j^2}{\pi\sqrt{\tau}_1} \left\{ \arg\left(1 + \dfrac{1}{\tau_1} \left(\lambda \tan\dfrac{k_1\pi}{2\alpha} \right) \right) \right. \\ \qquad \left. - \arg\left(1 - \dfrac{1}{\tau_1} \left(\lambda \tan\dfrac{k_1\pi}{2\alpha} \right) \right) \right\} \\ \qquad \text{if } \hbar\omega < \varepsilon_{\mathrm{CBM}}. \end{cases} \tag{7}$$

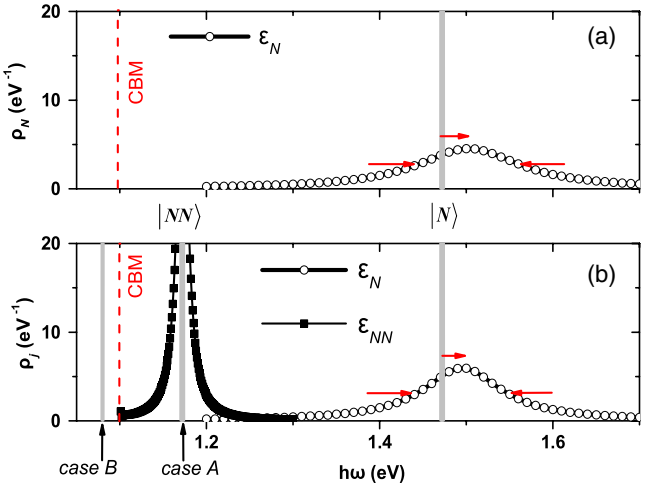

Figure 1. Density distribution of localized states (a) for SIAM and (b) for MIAM. In (a) and (b) grey stands for unmixed dispersionless impurity levels and red dashed line for CBM of InGaAs. In (b), in case A, the mixed pair/cluster state has small broadening ($\Delta_{NN} = 15$ meV) and remains practically unshifted ($\Lambda_{NN} = 0.4$ meV), whereas in case B, it neither broadens nor shifts. For single nitrogen, it is $2\Delta_N = 107$ meV and $\Lambda_N = 23$ meV.

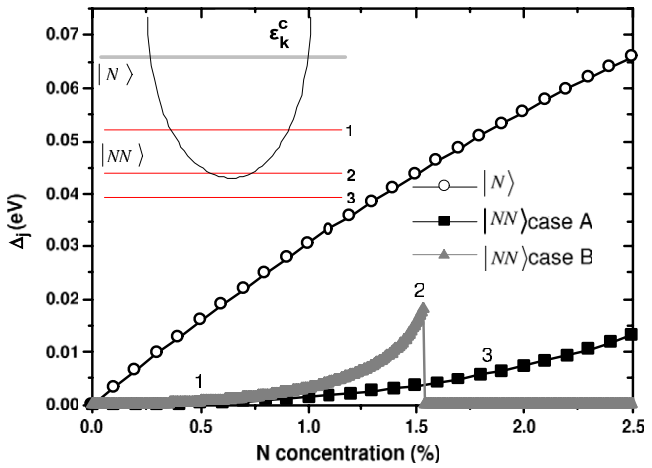

Figure 2. Broadening of impurity states Δ_j versus nitrogen concentration for MIAM. In case A (solid squares) pair/cluster states are above the CBM of InGaAs for all nitrogen concentrations, and their broadening increases monotonically. In case B (grey triangles), numbers 1, 2, 3 correspond to the position of pair/cluster states in relation to the CBM as shown in the inlet. Biggest broadening is observed when they are quasi-resonant with the CBM, due to largest interaction at that point. In position 3 they act as truly bound states with infinite scattering cross-section (at $T = 0$).

with $\tau_1 = C_b^2 - (C_a - \hbar\omega)^2$ and $\lambda = C_a - C_b - \hbar\omega$. The poles of the $|j\rangle$ states are now defined through $\Lambda_j(\hbar\omega)$ as

$$\overline{\hbar\omega_j} = \varepsilon_j + \Lambda_j(\hbar\omega). \tag{8}$$

The imaginary part $\Delta_j(\hbar\omega)$ of equation (6), which is related to the impurity broadening, is

$$-\operatorname{Im}[\Sigma_{\text{ret}}(\hbar\omega)] = |\Delta_j(\hbar\omega)| = \alpha\frac{V_j^2}{\tau_1^{1/2}} \tag{9}$$

where τ_1 was given in equation (7). $\Delta_j(\hbar\omega)$ is defined as half of the width of the spectral distribution of the impurity, which has a Lorentzian lineshape due to its finite lifetime

$$\rho_j(\hbar\omega) = \frac{1}{\pi}\frac{\Delta_j(\hbar\omega)}{(\hbar\omega - \varepsilon_j - \Lambda_j(\omega))^2 + \Delta_j(\hbar\omega)^2}. \tag{10}$$

Figure 1(a) shows the spectral distribution of the impurity level before and after mixing in the SIAM case. Figure 1(b) shows the spectral distribution for two generic MIAM cases: case A: with the second level |NN⟩ above the conduction band minimum and case B: with the second level below the conduction band minimum (CBM). The two cases are of interest as they result in different effective masses at the conduction band minimum, hence different densities of states. In the former case the pair/cluster level interacts with the conduction band and the level is shifted slightly and broadened, while in the latter for the pair/cluster state the interaction goes to zero, acting as a strong scattering resonance. Figure 2 shows the broadening of each impurity state as a function of the nitrogen composition. We have assumed the two generic cases A and B for a 8 nm QW of $Ga_{0.68}In_{0.32}N_{0.02}As_{0.98}$/GaAs. Based on Healy's *et al* formulation [6], we assume $\varepsilon_N = 1.55 - 3.9y$, where y is the total nitrogen concentration. For case A, $\varepsilon_{NN} = 1.25 - 3.9y$ which implies that pairs will always lie above the CBM (for N = 2.5% they are quasi-resonant with an energy distance of 52.3 meV). For case B, $\varepsilon_{NN} = 1.159 - 3.9y$ which means that for N = 1.52%, $\varepsilon_{CBM} = \varepsilon_{NN}$. We conclude that the interaction is stronger when the impurities are close to the conduction band minimum and when their concentration is high.

2.3. Method of solution: the conduction levels—general

Conduction band Green's functions are used to describe how the perturbed $|s'\rangle$ states are altered after mixing [8–11, 13]. Regarding this, our approach differs in the sense that we use the assumptions and the results from section 2.2 for the fitting function [21] and for the broadening of the impurity states (equation (9)). The way the relative position of the pair/cluster states to the minimum of the conduction band, affects the mixed states is also examined here.

The Green's function for the conduction band is given by [20]

$$G_k(\hbar\omega) = \left\{\hbar\omega - \varepsilon_k^c - \sum_j \frac{V_j^2}{\hbar\omega - \varepsilon_j + \mathrm{i}\Delta_j}\right\}^{-1}. \tag{11}$$

Equation (11) yields three poles; the real and imaginary parts represent the energy dispersion and the broadening of the mixed subbands respectively. For MIAM, contrary to SIAM [21], it is more difficult to obtain analytical solutions for these states. The complex solutions of equation (11) are

$$\hbar\omega_1 = \frac{1}{3}\left(C_1(y,k) + \frac{2^{2/3}A_3(y,k) - A_5^{2/3}(y,k)}{2^{1/3}A_5^{1/3}(y,k)}\right) \tag{12}$$

$$\hbar\omega_2 = \tfrac{1}{3}\left(C_1(y,k) - \frac{2^{2/3}(1+\mathrm{i}\sqrt{3})A_3(y,k) - (1-\mathrm{i}\sqrt{3})A_5^{2/3}(y,k)}{2^{4/3}A_5^{1/3}(y,k)}\right) \tag{13}$$

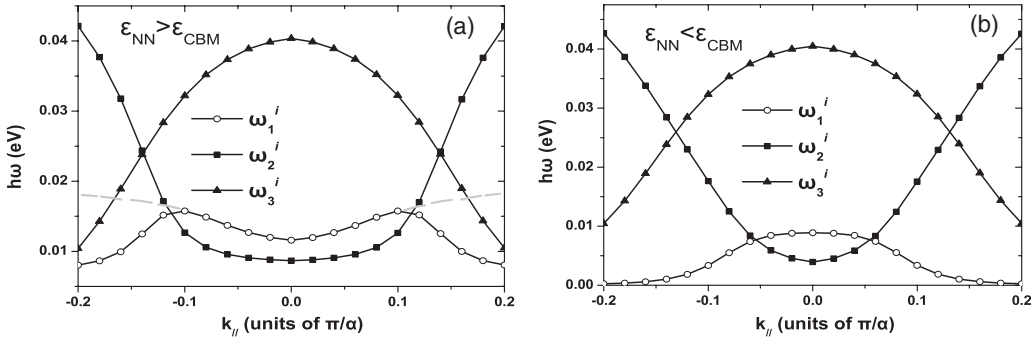

Figure 3. Broadening ω_1^{i}, ω_2^{i}, ω_3^{i} of the perturbed $|s'\rangle$ eigenstates ω_1^{r}, ω_2^{r}, ω_3^{r} correspondingly, for N = 2% for (a) case A, ($\varepsilon_{\mathrm{NN}} > \varepsilon_{\mathrm{CBM}}$) and (b) case B, ($\varepsilon_{\mathrm{NN}} < \varepsilon_{\mathrm{CBM}}$). The magnitude of the broadening is linked with the percentage of localized nitrogen character $1 - |\Gamma_c|^2$, which depends on the coupling parameter and on the energy separation between localized and delocalized states. The dashed grey lines in (a) indicate the broadening ω_2^{i} for N > 2%.

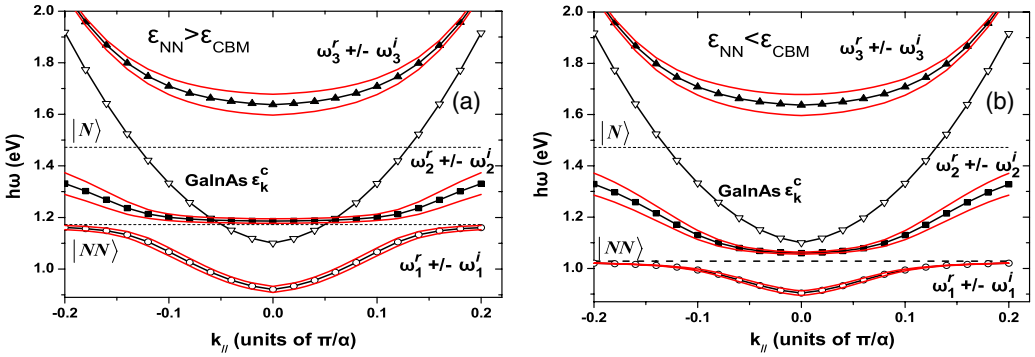

Figure 4. Complex conduction band structure of $Ga_{0.68}In_{0.32}N_{0.02}As_{0.98}$ when (a) $\varepsilon_{\mathrm{NN}} > \varepsilon_{\mathrm{CBM}}$ and (b) $\varepsilon_{\mathrm{NN}} < \varepsilon_{\mathrm{CBM}}$. The perturbed $|s'\rangle$ eigenstates are ω_1^{r}, ω_2^{r}, ω_3^{r} with their corresponding broadenings (figure 3) shown with red satellite lines. The localized character of $|s'\rangle$ is dependent on the strength of the interaction between the localized and the delocalized states and on the energy difference $|\varepsilon_j - \omega_t^{\mathrm{r}}|$ ($t = 1, 2, 3$) and is expressed by enhanced broadening.

$$\hbar\omega_3 = \frac{1}{3}\left(C_1(y,k) - \frac{2^{2/3}(1-\mathrm{i}\sqrt{3})A_3(y,k) - (1+\mathrm{i}\sqrt{3})A_5^{2/3}(y,k)}{2^{4/3}A_5^{1/3}(y,k)}\right) \quad (14)$$

where $C_1 = \varepsilon_k^{\mathrm{c}} + \varepsilon_{\mathrm{N}} + \varepsilon_{\mathrm{NN}} + \mathrm{i}(\Delta_{\mathrm{N}} + \Delta_{\mathrm{NN}})$ and $\hbar\omega_1$, $\hbar\omega_2$, $\hbar\omega_3$ correspond to the lower, middle and upper restructured subbands respectively. Parameters A_3 and A_5 are given in the appendix. In principle, analytical solutions for the real and for the imaginary component can be derived, but their form is not easily manipulated and their presentation exceeds the scope of this paper.

2.4. Method of solution: the conduction levels—QW $Ga_{1-x}In_xN_yAs_{1-y}$/GaAs case

We examine again the behaviour of an 8 nm QW system for cases A and B. In the following calculations we assume one confined state neglecting any higher lying ones. The energy broadening, which is depicted in figure 3, is associated with the projection of $|j\rangle$ states on the mixed $|s'\rangle$ and corresponds to the imaginary components of equations (12)–(14). For simplicity we will represent the solutions $\hbar\omega_1$, $\hbar\omega_2$, $\hbar\omega_3$ respectively as ω_1, ω_2, ω_3. In both cases, upper state ω_3^{r} is localized nitrogen-like near $k_\parallel = 0$ and more conduction band-like at higher $k_\parallel$. Interaction of middle state ω_2^{r} with single nitrogen state down the in-plane vector, results in increasing broadening ω_2^{i} (for both cases A and B). Also, the lowest state ω_1^{i} is bigger in case A than in case B, where the broadening drops quickly after $k_\parallel \sim 0.07\pi/\alpha A^{-1}$, as the admixture component $\langle\psi_{\mathrm{NN}}|\widehat{H}|\phi_{\mathrm{k}}^{\mathrm{c}}\rangle$ does not contribute in the calculation. Finally, ω_2^{i} increases faster along the plane vector in case B, which is attributed to the repelling forces on ω_2^{r} arising from the localized states. In comparison to SIAM [21], broadenings here are smaller about 10–35 meV for each one of the mixed states, but if they are all summed, the total broadening is maintained. The full conduction band structure for both cases in shown in figure 4. This has been compared in detail with the BAC model in [21]. There is significant difference in the energy dispersion ω_1^{r} between cases A and B, which is important, as this is related to the variation of the effective mass with further implications on the density of states.

Using tight-binding calculations and LCINS [8] the fractional Γ_1^{c} character of the perturbed subbands at the CBM has been shown to vary in a non-monotonical way, following the variation of the effective mass, m_{eff}. It is also interesting to see how Γ_1^{c} varies as a function of the reciprocal **k** vector. The fractional Γ_1^{c} character has been given by Vaughan and

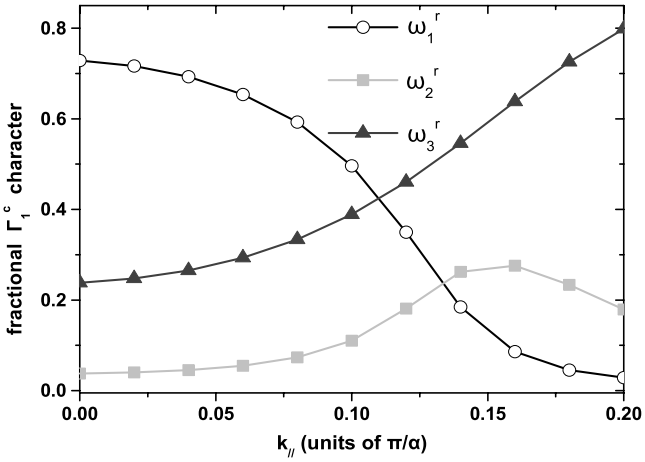

Figure 5. Fractional Γ_1^c character of the mixed subbands versus the in-plane $k_{||}$ vector for N = 2%. Behaviour can be easily explained by looking also at the broadenings in figure 3 and the dispersion profile in figure 4.

Ridley [13] as

$$\Gamma_1^c = \left[\sum_j \frac{V_j^2}{(\varepsilon_j - \hbar\omega)^2 + [\Delta_j - \Delta(\hbar\omega)]^2} + 1\right]^{-1}. \quad (15)$$

The broadening term in the denominator has a very small effect in the final outcome. Using our previous results as input parameters, it is straightforward to extract information for Γ_1^c for each subband. To do so, the term $\hbar\omega$ in the denominator is replaced by the real parts ω_1^r, ω_2^r, ω_3^r from equations (12)–(14) and the broadening $\Delta(\hbar\omega)$ by the imaginary parts ω_1^i, ω_2^i, ω_3^i of the same set of equations. Figure 5 shows the dependence of Γ_1^c on reciprocal vector when $\varepsilon_{NN} > \varepsilon_{CBM}$ as in figure 4(a). Based on information from figure 5 and the bandstructure from figure 4, it is easy to associate the variation of Γ_1^c with energy $\hbar\omega$. This is important because Γ_1^c enters the expression of nitrogen induced scattering mechanism $w_N(\hbar\omega)$ in bulk and QW structures in dilute nitrides [13, 15].

3. The density of states

It is interesting to see how the density of states N_D in the dilute nitride system is modified due to the strong perturbation arising from the nitrogen impurities. The density of states cannot be derived using the effective mass m_{eff} as this goes to infinity after mixing. The density of states N'_D is derived using the imaginary part of the Green's functions [11, 12] giving

$$N'_{tD} = -\frac{1}{\pi}\,\mathrm{Im}\int G_k(\hbar\omega) N_{tD}(\varepsilon_k^c)\mathrm{d}\varepsilon_k^c \quad (16)$$

where t refers to the unconfined dimensions. Using the following definitions

$$A(y,\hbar\omega) = \hbar\omega - \sum_j \frac{(\hbar\omega - \varepsilon_j(y))V_j^2(y)}{(\hbar\omega - \varepsilon_j(y))^2 + \Delta_j^2(y)} \quad (17)$$

$$B(y,\hbar\omega) = -\sum_j \frac{V_j^2(y)\Delta_j(y)}{(\hbar\omega - \varepsilon_j(y))^2 + \Delta_j^2(y)}. \quad (18)$$

$\mathrm{Im}\, G_k(y,\hbar\omega)$ can be written as

$$\mathrm{Im}\, G_k(y,\hbar\omega) = -\frac{B(y,\hbar\omega)}{[A(y,\hbar\omega) - \varepsilon_M]^2 - B(y,\hbar\omega)^2} \quad (19)$$

where ε_M is the energy at CBM. Inserting equation (19) in equation (16) we derive slightly different expressions (from [13]) for the perturbed DOS:

$$N'_{3D}(\hbar\omega) = -\frac{1}{4\pi^2}\left(\frac{2m_{eff}}{\hbar^2}\right)^{3/2} \times \frac{A(y,\hbar\omega)\sin\theta + B(y,\hbar\omega)\cos\theta}{\{A^2(y,\hbar\omega) + B^2(y,\hbar\omega)\}^{1/4}} \quad (20)$$

$$N'_{2D}(\hbar\omega) = \frac{m_{eff}}{2\pi\hbar^2}\left(\frac{1}{2} - \frac{1}{\pi}\arctan\left[\frac{A(y,\hbar\omega) - \varepsilon_n}{B(y,\hbar\omega)}\right]\right) \quad (21)$$

where $\theta = \frac{1}{2}\arg[-A(y,\hbar\omega) + iB(y,\hbar\omega)]$. The 1D DOS is given by

$$N'_{1D}(\hbar\omega) = -\frac{m_{eff}}{2\pi\hbar}\frac{\sin\theta}{\{A^2(y,\hbar\omega) + B^2(y,\hbar\omega)\}^{1/4}}. \quad (22)$$

Figure 6 shows the 3D (3 dimension) (bulk), 2D (QW) and 1D (QWW) perturbed density of states for two nitrogen concentrations of 0.5% and 2.5%, assuming both a variable broadening Δ_j (dependent on nitrogen concentration) and a constant one. The variable broadening stems, as explained in section 2.1, from the assumption of multiple scattering by the same impurity. Here we test the implications of our assumption on the density of states by comparing them with previous results that consider a fixed Δ_j [12, 13].

First of all in both cases, the density of states exhibit the same trends; two distinct peaks at the nitrogen impurity levels whilst far from them they tend to reshape to the parent density of states, depicted with grey line. The peaks are redshifted with increasing nitrogen because their position depends on the nitrogen concentration and because the strength of the interaction increases, shifting their position after mixing. Also, for all structures, at lower energies, there is a band tailing of the density of states observed in the bandgap. Finally, the only qualitative difference between the 3D, 1D and 2D case is that in the latter no singularity-like characteristics are observed at the impurity levels.

Comparing now in figure 6 the two approaches of a variable (calculated) and a fixed broadening with nitrogen concentration we observe that they are in very good agreement. There is however some deviation observed at the impurity energy levels. For fixed broadening of the impurity (here we assume that $\Delta_N = 50$ meV, $\Delta_{NN} = 20$ meV) the characteristic peaks of the mixed DOS (observed at impurity level energies) scale with nitrogen concentration. In other words, we observe in all three graphs of figure 6 a very small feature for N = 0.5% and a much more distinct one for N = 2.5%. On the other hand, we see that our approach of calculated broadening ($\Delta_N = 15$ meV, $\Delta_{NN} = 3$ meV for N = 0.5% and $\Delta_N = 66$ meV, $\Delta_{NN} = 13$ meV for N = 2.5%) gives somewhat different characteristics; for all structures the peak at the single nitrogen level ($\hbar\omega \simeq 1.5$ eV) has almost the same magnitude for small and high nitrogen. This may seem odd at a first sight and the intuitive question of why the peak

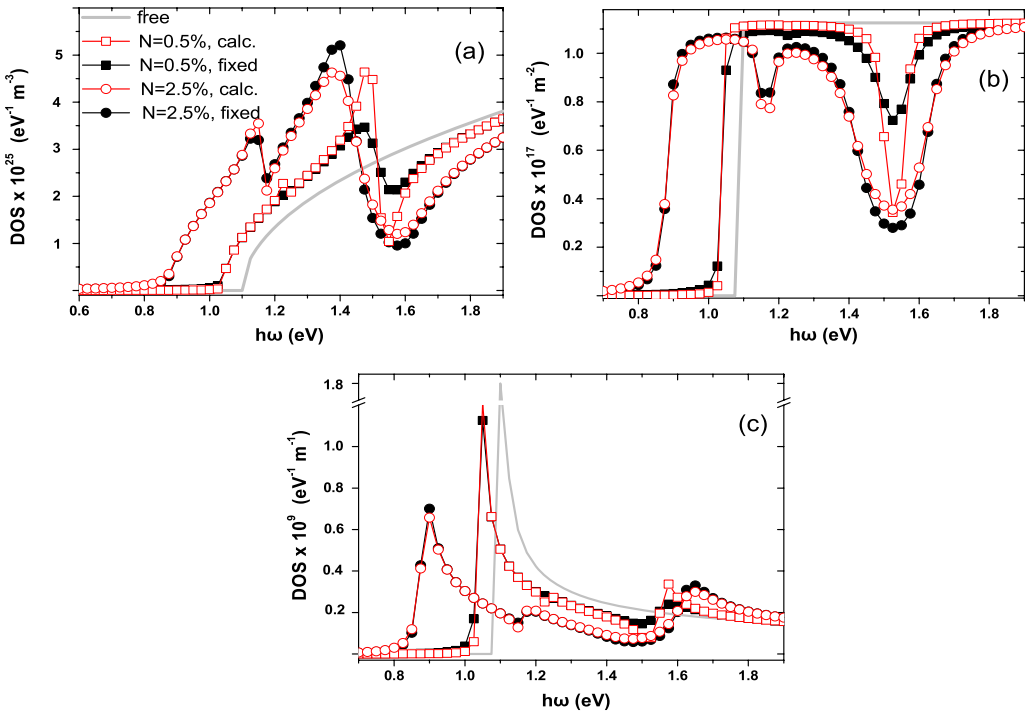

Figure 6. Restructured DOS in the (a) bulk, (b) QW and (c) QWW case for N = 0.5% and 2.5%. Lines in (b) and (c) follow the notation of label in (a). 'Fixed' and 'calc' refer to the fixed and the calculated broadening of the impurity states, respectively. Grey lines with no symbol refer to the parent InGaAs DOS. The fixed broadening here is $\Delta_N = 50$ meV and $\Delta_{NN} = 20$ meV whilst the calculated for N = 0.5% is $\Delta_N = 15$ meV, $\Delta_{NN} = 3$ meV and for N = 2.5% is $\Delta_N = 66$ meV, $\Delta_{NN} = 13$ meV. Severe distortion at the impurity levels and band tailing inside the band gap is observed. Despite the small difference in shape between the two approaches at the impurity levels, the area of the DOS under the curves remains exactly the same.

for small nitrogens does not smear out, may physically arise. As has been pointed out before in this section, this is a feature that comes out naturally based on the assumption of multiple scattering. However, we believe that the figure of merit for the validity of the assumption should be the integrated density of states and not their absolute magnitude at the impurity levels.

We have calculated the integrated density of states and a deviation between the two approaches of less than 1% on average has been found for three nitrogen concentrations (0.5%, 1.5%, 2.5%) for all 3D, 2D and 1D structures. The integration has been carried out both in the vicinity of the impurity levels and in the whole energy spectrum depicted in figure 6. For example, it is clear in figures 6(a) and (b) that at the single nitrogen level the peak for calculated broadening is more prominent but at the same time its width is smaller than that of fixed broadening. Therefore, we believe that the two approaches are in qualitative and quantitative agreement.

In case of high localization, in other words for $\Delta_j \to 0$ the density of states at the impurity level becomes infinitely high, which is physically reasonable.

Knowledge of the exact density of states is important since it enables us to proceed with calculations on optical properties and on carrier transport in 2D and 3D GaInNAs structures.

4. Discussion and conclusions

We have used the SIAM and extended it to derive a MIAM to describe the GaInNAs material system in bulk and confined geometries. We have used the Matsubara Green's function approach to derive analytical expressions for mixed conduction band and N impurity levels in the system. Using a fitting function for the parabolic conduction band of InGaAs and using multiple scattering by one impurity we have derived analytical expressions for: the mixed impurity levels, the conduction band structure and the density of states. Nitrogen impurities are found to change drastically the shape of the parent DOS. The information gained using this approach goes beyond that obtained from the usual BAC model. We have explicitly treated two different cases, based on the energy position of the N–N pair/cluster states relative to the conduction band minimum and have shown how this affects the system's behaviour. Also, it is straightforward to compare the results on the band structure derived from the MIAM to those derived from the BAC model and see that they are in a general agreement.

We approximate the distribution of pair and cluster states by one averaged energy level in this model. By extending the MIAM we could consider a number of levels within the distribution but we believe that by varying the energy level within this range we have essentially explored the importance of the energy levels within the distribution. Energy levels closest to the conduction band minimum are observed to have the strongest effect. We have used various distribution types to approximate the more realistic non-symmetrical distribution of the impurity levels [5, 23]. It is valid to say that we can model a non-symmetrical distribution with one effective level,

if this is recalculated with an effective mean (weighted by the probability at each energy). In this meta-stable system the actual concentration of each type of state will be changed upon growth and may be controlled through growth or post annealing [18]. The aim of this paper was to understand how the level of these states influences the bandstructure and DOS. We have also used spatially averaged interaction strength within this model. For confined systems the interaction strength will depend on the overlap of the wavefunction of the confined conduction band level with the nitrogen defect and will be larger if the nitrogen can be placed in the centre of the QW or QWW [18]. Currently site position of nitrogen impurities cannot be controlled so site-averaging is appropriate.

The density of states is important for the analysis of optical and transport studies. In transport studies the electron scattering from an alloy is often calculated considering scattering from one crystal and considering the replacement atom to scatter the electron [17]. In this treatment this does not happen as the electron eigenstates of the coupled system already account for the incorporation of nitrogen into random lattice sites. The effect of this is the band gap shrinkage and altered effective mass. However, non-randomly situated nitrogen atoms and interstitial nitrogen atoms are still able to scatter the electrons and must be therefore considered. In the evaluation of scattering processes (e-phonon, e-defect) in the restructured $Ga_{1-x}In_xN_yAs_{1-y}$ system we should make use of the new DOS [16] (section 3) rather than the parabolic one of the host matrix. In optical studies the density of states is reflected in material gain which may be tuned for broad band or other applications using this approach.

Acknowledgment

The authors wish to thank Dr Bob Ren for useful comments on the manuscript.

Appendix. Parameters of the eigenstate expressions of 3 BAC model

The parameters A_3 and A_5 of equations (12)–(14) are given below.

$$\begin{aligned} A_3(y,k) = {} & -C_1^2(y,k) - 3\{-\varepsilon_k^{\mathrm{c}}(\varepsilon_{\mathrm{N}}+\varepsilon_{\mathrm{NN}}) \\ & - \varepsilon_{\mathrm{N}}\varepsilon_{\mathrm{NN}} + V_{\mathrm{N}}^2 + V_{\mathrm{NN}}^2 + \Delta_{\mathrm{N}}\Delta_{\mathrm{NN}} \\ & - \mathrm{i}[\Delta_{\mathrm{N}}(\varepsilon_k^{\mathrm{c}}+\varepsilon_{\mathrm{NN}}) + \Delta_{\mathrm{NN}}(\varepsilon_k^{\mathrm{c}}+\varepsilon_{\mathrm{N}})]\} \end{aligned} \tag{A.1}$$

$$A_5(y,k) = A_4(y,k) + \sqrt{4A_3^3(y,k) + A_4^2(y,k)} \tag{A.2}$$

where $C_1 = \varepsilon_k^{\mathrm{c}} + \varepsilon_{\mathrm{N}} + \varepsilon_{\mathrm{NN}} + \mathrm{i}(\Delta_{\mathrm{N}} + \Delta_{\mathrm{NN}})$ and

$$\begin{aligned} A_4(y,k) = {} & -2(\varepsilon_k^{\mathrm{c}3} + \varepsilon_{\mathrm{N}}^3 + \varepsilon_{\mathrm{NN}}^3) + 3A_1(y,k) \\ & + 3\mathrm{i}A_2(y,k) + 2\mathrm{i}(\Delta_{\mathrm{N}}^3 + \Delta_{\mathrm{NN}}^3) \end{aligned} \tag{A.3}$$

where

$$\begin{aligned} A_1(y,k) = {} & \varepsilon_k^{\mathrm{c}2}(\varepsilon_{\mathrm{N}}+\varepsilon_{\mathrm{NN}}) + \varepsilon_k^{\mathrm{c}}\varepsilon_{\mathrm{N}}^2 - \varepsilon_{\mathrm{N}}\varepsilon_{\mathrm{NN}}(4\varepsilon_k^{\mathrm{c}} - \varepsilon_{\mathrm{N}}) \\ & + \varepsilon_{\mathrm{NN}}^2(\varepsilon_k^{\mathrm{c}}+\varepsilon_{\mathrm{N}}) - 3V_{\mathrm{N}}^2(\varepsilon_k^{\mathrm{c}}+\varepsilon_{\mathrm{N}}-2\varepsilon_{\mathrm{NN}}) \\ & - 3V_{\mathrm{NN}}^2(\varepsilon_k^{\mathrm{c}}-2\varepsilon_{\mathrm{N}}+\varepsilon_{\mathrm{NN}}) - \Delta_{\mathrm{N}}^2(\varepsilon_k^{\mathrm{c}}-2\varepsilon_{\mathrm{N}}+\varepsilon_{\mathrm{NN}}) \\ & + \Delta_{\mathrm{N}}\Delta_{\mathrm{NN}}(4\varepsilon_k^{\mathrm{c}} - 2\varepsilon_{\mathrm{N}} - 2\varepsilon_{\mathrm{NN}}) - \Delta_{\mathrm{NN}}^2(\varepsilon_k^{\mathrm{c}}+\varepsilon_{\mathrm{N}}-2\varepsilon_{\mathrm{NN}}) \end{aligned} \tag{A.4}$$

and

$$\begin{aligned} A_2(y,k) = {} & \varepsilon_k^{\mathrm{c}}\Delta_{\mathrm{N}}(\varepsilon_k^{\mathrm{c}}+2\varepsilon_{\mathrm{N}}) - 2\Delta_{\mathrm{N}}(\varepsilon_{\mathrm{N}}^2 + 2\varepsilon_k^{\mathrm{c}}\varepsilon_{\mathrm{NN}} - \varepsilon_{\mathrm{N}}\varepsilon_{\mathrm{NN}}) \\ & + \Delta_{\mathrm{N}}(\varepsilon_{\mathrm{NN}}^2 - 3V_{\mathrm{N}}^2 + 6V_{\mathrm{NN}}^2) + \Delta_{\mathrm{NN}}(\varepsilon_k^{\mathrm{c}2} + \varepsilon_{\mathrm{N}}^2) \\ & + 2\varepsilon_k^{\mathrm{c}}\Delta_{\mathrm{NN}}(\varepsilon_{\mathrm{NN}} - 2\varepsilon_{\mathrm{N}}) + 2\varepsilon_{\mathrm{NN}}\Delta_{\mathrm{NN}}(\varepsilon_{\mathrm{N}} - \varepsilon_{\mathrm{NN}}) \\ & + 3\Delta_{\mathrm{NN}}(2V_{\mathrm{N}}^2 - V_{\mathrm{NN}}^2) - \Delta_{\mathrm{N}}\Delta_{\mathrm{NN}}(\Delta_{\mathrm{N}} - \Delta_{\mathrm{NN}}). \end{aligned} \tag{A.5}$$

References

[1] Kondow M, Uomi K, Niwa A, Kitatani T, Watahiki S and Yazawa Y 1996 *Japan. J. Appl. Phys.* **35** 1273
[2] Weyers M, Sato M and Ando H 1992 *Japan. J. Appl. Phys.* **31** 853
[3] Shan W, Walukiewicz W, Ager J W III, Haller E E, Geisz J F, Friedman D J, Olson J M and Kurtz S R 1999 *Phys. Rev. Lett.* **82** 1221
[4] Liu X, Pistol M E, Samuelson L, Schwetlick S and Seifert W 1990 *Appl. Phys. Lett.* **56** 1451
[5] Lindsay A and O'Reilly E P 2004 *Phys. Rev. Lett.* **93** 196402
[6] Healy S B, Lindsay A and O'Reilly E P 2004 *IEE Proc., Optoelectron.* **151** 397
[7] Kent P R C and Zunger A 2001 *Phys. Rev. Lett.* **86** 2613
[8] O'Reilly E P, Lindsay A and Fahy S 2004 *J. Phys.: Condens. Matter* **16** 3257
[9] Mahan G D 1990 *Many Particle-Physics* (New York: Plenum) p 133
[10] Zubarev D N 1960 *Sov. Phys.—Usp.* **3** 320
[11] Elliott R J, Krumhans J A and Leath P L 1974 *Rev. Mod. Phys.* **46** 465
[12] Wu J, Shan W and Walukiewicz W 2002 *Semicond. Sci. Technol.* **17** 860
[13] Vaughan M P and Ridley B K 2007 *Phys. Rev.* B **75** 195205
[14] Anderson P W 1961 *Phys. Rev.* **124** 41
[15] Fahy S, Lindsay A, Ouardane H and O'Reilly E P 2006 *Phys. Rev.* B **74** 035203
[16] Vogiatzis N, Qiu Y N and Rorison J M 2008 *Proc. SPIE* **6997** 69971V
[17] Littlejohn M A, Hauser J R, Glisson T H, Ferry D K and Harrison J W 1978 *Solid-State. Electron.* **21** 107
[18] Qiu Y N and Rorison J M 2005 *Appl. Phys. Lett.* **87** 081111
[19] Ulloa J M, Snches-Rojas J L, Hierro A, Tijero J M and Tourni E 2005 *IEEE J. Quantum Electron.* **9** 716
[20] Vaughan M P 2007 *PhD Thesis* University of Essex
[21] Vogiatzis N and Rorison J M 2008 *Phys. Status Solidi* a **205** 120
[22] Lindsay A and O'Reilly E P 1999 *Solid State Commun.* **112** 443
[23] Polimeni A *et al* 2008 *Phys. Rev.* B **77** 155213